Directing the Architecture of Various MoS_2 Hierarchical Hollow Cages through the Controllable Synthesis of Surfactant/Molybdate Composite Precursors

Lina Ye, Wen Guo, Ye Yang, Yongfang Du, and Yi Xie*

Department of Nanomaterials and Nanochemistry, Hefei National Laboratory for Physical Sciences at Microscale, University of Science and Technology of China, Hefei 230026, P. R. China

Received July 25, 2007. Revised Manuscript Received September 30, 2007

We proposed a general route to MoS_2 hierarchical hollow cages, in which abundant hollow cages with various well-defined, novel geometrical morphologies were fabricated via a self-assembly coupled with surfactant/molybdate composite precursor crystal templating process based on the Kirkendall Effect. The in situ formed surfactant/molybdate composite precursor crystals with cubic structures, which are cooperatively assembled by periodic Mo oxo anion and tetrabutylammonium cation, play crucial roles as both the Mo source and the template in the formation of MoS_2 hierarchical hollow cages. Various morphologies of the surfactant/molybdate composite precursor crystals were controllably synthesized through a methodical tuning of the habit and the degree of branching of precursor crystals by varying the SCN^- concentration and surfactant concentration.

1. Introduction

Hierarchical hollow nanostructures are useful in applications such as catalysis, drug delivery, lightweight filter, acoustic insulation, photonic crystals,[1] and so on. However, in most cases, only spherical hierarchical hollow structures could be synthesized through the use of emulsion droplets[2] as templates or by direct self-assembly of primary particles.[3–5] Recently, through different synthetic strategies, some anisotropic hierarchical hollow inorganic nanostructures with regular morphologies such as rhombododecahedral silver cages,[6] cubic MoS_2 cages,[7] and octahedral and cubic $Cu_{2-x}Se$ cages[8] have been prepared; however, only a few specific forms of the hierarchical hollow cages could be synthesized through different synthetic strategies.[2–8] Thus, it is desirable to explore facile methods to systematically synthesize hollow cages with various well-defined, novel geometrical morphologies.

Our earlier work confirms that micrometer-scaled MoS_2 hierarchical hollow cubic cages assembled by bilayers can be synthesized via a one-step self-assembly coupled with $K_2NaMoO_3F_3$ crystal templating process based on the Kirkendall effect.[7] From that we find the fabrication of hierarchical hollow structures mainly involves the following three key points: (a) the intermediate crystals formed in situ, which would act as the precursor and template for the further reaction; (b) a morphology-preserved MoS_2 shell formed; (c) continuous evacuation of template crystal core led to the formation of hollow MoS_2 cages. Enlightened by this templating process based on the Kirkendall effect, we therefore suppose, by controlling the morphology of the in situ formed precursor template crystals, we could controllably synthesize various MoS_2 hierarchical hollow cages with special morphologies. Although it is extensively accepted that the concentrations of reactants are likely to alter the habit formation and the branching growth of the precursor crystals, our succedent research indicates that it is difficult to modify the morphology of the in situ formed $K_2NaMoO_3F_3$ crystal through simple manipulation, such as the addition of surfactants or the alteration of the concentration of reactants. Therefore, searching for a precursor crystal with more adjustable morphology is crucial to the controllable synthesis of various morphology-preserved MoS_2 hollow cages. Fortunately, we find an in situ formed surfactant/molybdate composite precursor crystal with cubic structures, which is cooperatively assembled by periodic Mo oxo anion and tetrabutylammonium cation, has more adjustable morphology, and could play crucial roles as both the Mo source and the template in the formation of MoS_2 hierarchical hollow cages. Herein we report a general route to MoS_2 hierarchical hollow cages in which abundant hollow cages with various well-defined, novel geometrical morphologies are controllably fabricated through a methodical tuning of the habit and the degree of branching of surfactant/molybdate composite precursor crystals by varying the concentration of reactants via a facile approach involving MoO_3, NaF, Bu_4NBr, and NaSCN.

* Corresponding author: Tel 86-551-3603987, Fax 86-551-3603987, e-mail yxie@ustc.edu.cn.

(1) Caruso, F. *Chem.—Eur. J.* **2000**, *6*, 413.
(2) Dinsmore, A. D.; Hsu, M. F.; Nikolaides, M. G.; Marquez, M.; Bausch, A. R.; Weitz, D. A. *Science* **2002**, *298*, 1006.
(3) Bigi, A.; Boanini, E.; Walsh, D.; Mann, S. *Angew. Chem., Int. Ed.* **2002**, *41*, 2163.
(4) Yuan, J.; Laubernds, K.; Zhang, Q.; Suib, S. L. *J. Am. Chem. Soc.* **2003**, *125*, 4966.
(5) Liu, B.; Zeng, H. C. *J. Am. Chem. Soc.* **2004**, *126*, 8124–8125.
(6) Yang, Y. J.; Qi, L. M.; Lu, C. H.; Ma, J. M.; Cheng, H. M. *Angew. Chem., Int. Ed.* **2005**, *44*, 598–603.
(7) Ye, L. N.; Wu, C. Z.; Guo, W.; Xie, Y. *Chem. Commun.* **2006**, 4738–4740.
(8) Cao, H.; Qian, X.; Zai, J.; Yin, J.; Zhu, Z. *Chem. Commun.* **2006**, 4548–4550.

10.1021/cm702007f CCC: $37.00
Published on Web 11/08/2007

2. Experimental Section

Preparation of MoS_2 Hierarchical Hollow Cages. NaF (0.006 mol), MoO_3 (0.003 mol), NaSCN (0.010–0.015 mol), and Bu_4NBr (0.0009–0.0018 mol) were added into 30 mL of distilled water and transferred to a 40 mL Teflon-lined strainless steel autoclave, which was then heated at 160 °C for 8 h and then 220 °C for 6 h in an electric oven. After reaction, the black precipitate was collected from the solution by centrifugation and washed with distilled water and anhydrous alcohol for several times. The final product was dried in a vacuum at 60 °C for 6 h.

Characterization. Powder X-ray diffraction (XRD) measurements of the samples were performed on a Japan Rigaku D/max rA X-ray diffractometer with Cu Kα radiation ($\lambda = 1.5418$ Å). The field emission scanning electron microscopy (FESEM) images were taken on a FEI Sirion-200 SEM. X-ray photoelectron spectra (XPS) was taken on ESCALAB 250 using monochromatic Al Kα radiation. X-ray fluorescence spectra (XFS), the Fourier transform infrared (FTIR), thermogravimetric analysis (TGA), element analysis, and inductively coupled plasma-atomic emission spectra (ICP-AES) were performed on XRF-1800, MAGNA-IR 750, DTG-60H, Elementar Vario EL-III, and Atomscan Advantage, respectively.

3. Results and Discussion

3.1. Structural Characterization and Morphological Evolution of MoS_2 Hierarchical Hollow Cages. Powder X-ray diffraction (XRD) patterns of these obtained MoS_2 hierarchical hollow cages are similar on the whole. The XRD pattern of the MoS_2 product obtained at 160 °C for 8 h and then at 220 °C for 6 h, with 0.01 mol of NaSCN and 0.0009 mol of Bu_4NBr (Figure S1) is consistent with a previous report[9] and indexes to hexagonal phase of MoS_2 with lattice parameters $a = 3.151(4)$ Å and $c = 12.78(6)$ Å, respectively.

Through the controllable synthesis of precursor crystals at different concentration of NaSCN and/or Bu_4NBr, we obtained various MoS_2 hierarchical hollow cages with well-defined, novel geometrical morphologies. For example, a series of the MoS_2 hollow cages based on a rhombododecahedral habit, as shown in Figure 1a, were grown from the solutions consisting of a constant amount of 0.01 mol of NaSCN and varying amount of Bu_4NBr (see caption of Figure 1a for detailed conditions). MoS_2 hierarchical hollow cages of rhombododecahedron (Figure 1a_1), rhombododecahedron with a total of 12 intracrystal holes on the centers of rhombic planes (Figure 1a_2), enlarged hexapod (Figure 1a_3), and hexapod (Figure 1a_4) can be prepared as the concentration of Bu_4NBr increases. Figure 2a shows low-magnification FESEM images of MoS_2 hierarchical hollow cages based on a rhombododecahedral habit to demonstrate the uniformity of morphology.

The other series of the MoS_2 hollow cages based on an 18-face polyhedral habit, as shown in Figure 1b, were grown from the solutions consisting of a constant amount of 0.012 mol of NaSCN and varying amount of Bu_4NBr (see caption of Figure 1b for detailed conditions). MoS_2 hierarchical hollow cages of 18-face polyhedron (Figure 1b_1), 18-face polyhedron with a total of six intracrystal holes on the centers of square planes (Figure 1b_2), octa-18-face polyhedron (Figure 1b_3), and octa-rhombododecahedron (Figure 1b_4) can be obtained separately, as the concentration of Bu_4NBr increases. Figure 2b shows low-magnification FESEM images of MoS_2 hierarchical hollow cages based on an 18-face polyhedral habit to demonstrate the uniformity of morphology.

Another series of the MoS_2 hollow cages based on a cubic habit, as shown in Figure 1c, were grown from the solutions consisting of a constant amount of 0.015 mol of NaSCN and varying amount of Bu_4NBr (see caption of Figure 1c for

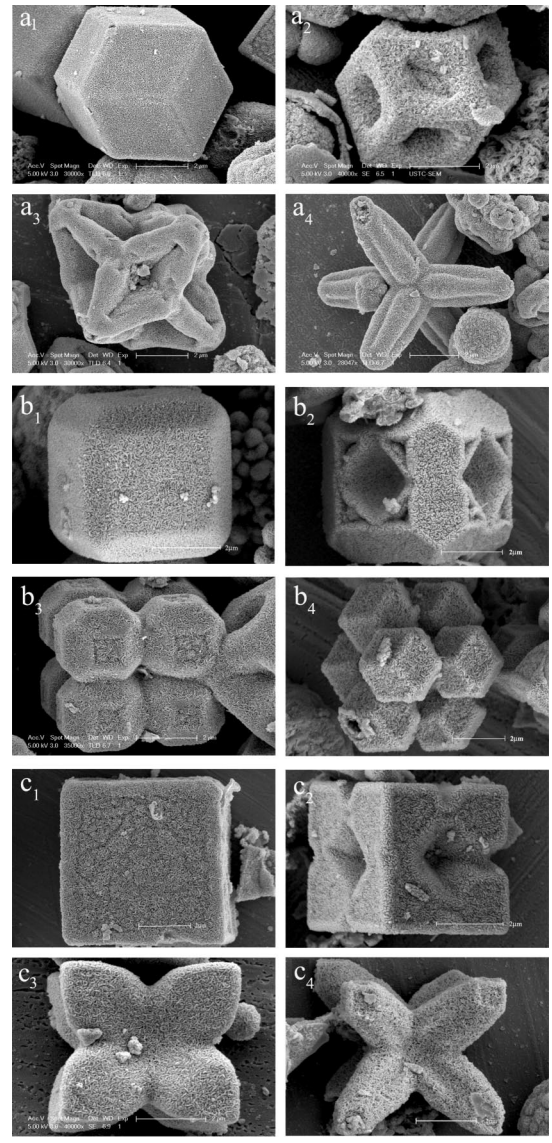

Figure 1. FESEM images of MoS_2 hierarchical hollow cages (a) based on rhombododecahedral habit but varying degrees of branching from solutions of a constant amount of 0.01 mol of NaSCN and varying amount of Bu_4NBr, of (a_1) 0.0009 mol of Bu_4NBr, (a_2) 0.00105 mol of Bu_4NBr, (a_3) 0.0012 mol of Bu_4NBr, and (a_4) 0.00128 mol of Bu_4NBr; (b) based on 18-face polyhedral habit but varying degrees of branching from solutions of a constant amount of 0.012 mol of NaSCN and varying amount of Bu_4NBr, of (b_1) 0.0009 mol of Bu_4NBr, (b_2) 0.00098 mol of Bu_4NBr, (b_3) 0.00105 mol of Bu_4NBr, (b_4) 0.0012 mol of Bu_4NBr; (c) based on cubic habit but varying degrees of branching from solutions of a constant amount of 0.015 mol of NaSCN and varying amount of Bu_4NBr, of (c_1) 0.0012 mol of Bu_4NBr, (c_2) 0.0015 mol of Bu_4NBr, (c_3) 0.00165 mol of Bu_4NBr, and (c_4) 0.0018 mol of Bu_4NBr. See Figure 2 for low-magnification FESEM images that show the uniformity of morphology for MoS_2 hierarchical hollow cages.

(9) Prasad, T. P.; Diemann, E.; Müller, A. *J. Inorg. Nucl. Chem.* **1973**, *35*, 1895–1904.

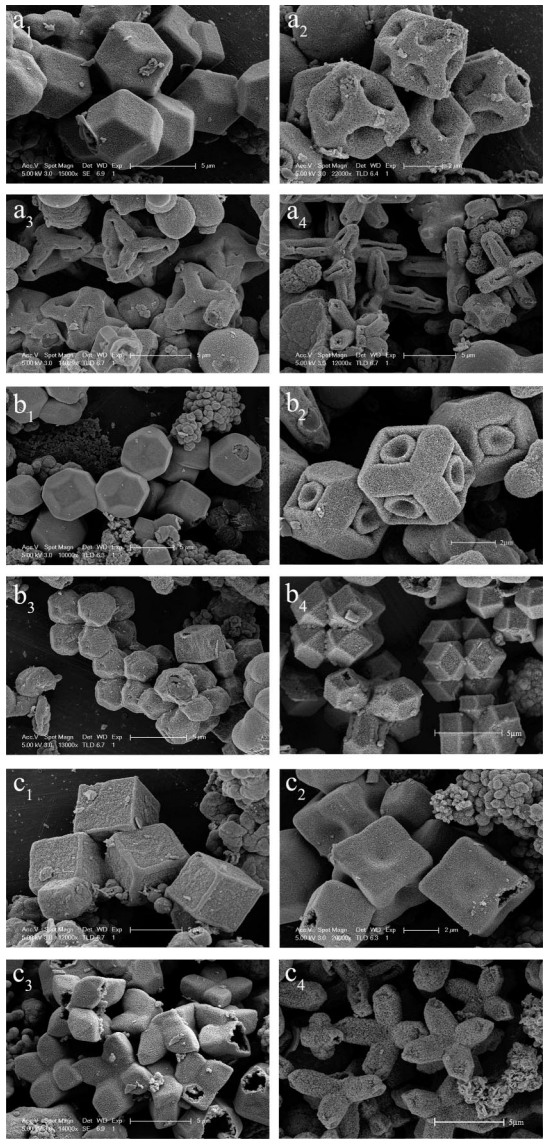

Figure 2. Low-magnification FESEM images of MoS_2 hierarchical hollow cages shown in Figure 1 to demonstrate the uniformity of morphology. Hollow cages: (a) based on rhombododecahedral habit but varying degrees of branching from solutions of a constant amount of 0.01 mol of NaSCN and varying amount of Bu_4NBr, of (a_1) 0.0009 mol of Bu_4NBr, (a_2) 0.00105 mol of Bu_4NBr, (a_3) 0.0012 mol of Bu_4NBr, and (a_4) 0.00128 mol of Bu_4NBr; (b) based on 18-face polyhedral habit but varying degrees of branching from solutions of a constant amount of 0.012 mol of NaSCN and varying amount of Bu_4NBr, of (b_1) 0.0009 mol of Bu_4NBr, (b_2) 0.00098 mol of Bu_4NBr, (b_3) 0.00105 mol of Bu_4NBr, and (b_4) 0.0012 mol of Bu_4NBr; (c) based on cubic habit but varying degrees of branching from solutions of a constant amount of 0.015 mol of NaSCN and varying amount of Bu_4NBr, of (c_1) 0.0012 mol of Bu_4NBr, (c_2) 0.0015 mol of Bu_4NBr, (c_3) 0.00165 mol of Bu_4NBr, and (c_4) 0.0018 mol of Bu_4NBr. The branching of the MoS_2 hierarchical hollow cages becomes more obvious as the concentration of Bu_4NBr increases.

detailed conditions). Cubic (Figure $1c_1$), dicelike (cube with a total of six intracrystal holes on the centers of square planes, Figure $1c_2$), enlarged octapod (Figure $1c_3$), and octapod (Figure $1c_4$) MoS_2 hierarchical hollow cages can be fabricated as the concentration of Bu_4NBr increases. Figure 2c shows low-magnification FESEM images of MoS_2 hierarchical hollow cages based on a cubic habit to demonstrate the uniformity of morphology.

From field emission scanning electron microscopy (FESEM) observations, we can find that this general strategy and facile route results in MoS_2 hollow cages with various well-defined, novel geometrical morphologies. All of the obtained MoS_2 cages are hollow in the interior, which can be clearly observed in some cracked cages; for example, the interior space of the hollow MoS_2 cages is clearly revealed on the FESEM image for an incomplete MoS_2 rhombododecahedral cage (Figure 3a). It can be seen from Figures 1 and 2 that all of the obtained MoS_2 hollow cages have an average size of about 5–6 μm and the shell of the cages consists of interconnected, irregularly shaped, primary nanoplates. As shown in an enlarged FESEM (Figure 3b), the shell of the cages consists of nanoplates about 100–200 nm in size.

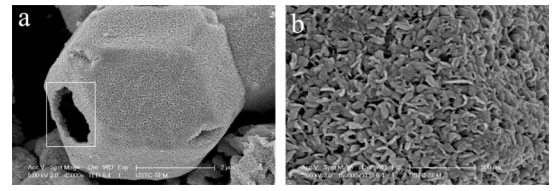

Figure 3. High-magnification FESEM images of rhombododecahedral MoS_2 hierarchical hollow cages: (a) a detailed view on an incomplete rhombododecahedral cage, from which we can see that its interior is hollow, as shown in the box above; (b) a detailed view on the surface of the rhombododecahedral cages, confirming that the shell of the cages consists of interconnected, irregularly shaped, primary nanoplates about 100–200nm in size.

3.2. Morphological Evolution and Structural Characterization of the Precursor Crystals. It has been revealed that the precursor crystals are crucial to the formation of morphology-preserved MoS_2 hollow cages. In order to investigate the formation mechanism of MoS_2 hierarchical hollow cages with different geometrical morphologies, the precursor crystals were captured for FESEM observations when the reactions were stopped at 160 °C for 8 h, exhibiting different morphologies from different systems as we expected. The precursor crystals obtained at a constant amount of 0.01 mol of NaSCN and varying amount of Bu_4NBr are ideal rhombododecahedron consisting of 12 well-defined crystal faces (at 0.0009 mol of Bu_4NBr, Figure $4a_1$), rhombododecahedron with a total of 12 intracrystal holes on the centers of rhombic planes (at 0.00105 mol of Bu_4NBr, Figure $4a_2$), enlarged hexapod (at 0.0012 mol of Bu_4NBr, Figure $4a_3$), and hexapod (at 0.00128 mol of Bu_4NBr, Figure $4a_4$), in accordance with their offspring of MoS_2 hollow cages in Figure 1a. The precursor crystals obtained at a constant amount of 0.012 mol of NaSCN and varying amount of Bu_4NBr are 18-face polyhedron (at 0.0009 mol of Bu_4NBr, Figure $4b_1$), 18-face polyhedron with a total of six intracrystal holes on the centers of square planes (at 0.00098 mol of Bu_4NBr, Figure $4b_2$), octa-18-face polyhedron (at 0.00105 mol of Bu_4NBr, Figure $4b_3$), and octa-rhombododecahedron (at 0.0012 mol of Bu_4NBr, Figure $4b_4$), consistent with their offspring of MoS_2 hollow cages in Figure 1b. The cubic (at 0.0012 mol of Bu_4NBr, Figure $4c_1$), dicelike (cube with a total of six intracrystal holes on the centers of square planes, formed at 0.0015 mol of Bu_4NBr, Figure $4c_2$), enlarged octapod (at 0.00165 mol of Bu_4NBr, Figure $4c_3$), and octapod (at 0.0018 mol of Bu_4NBr, Figure $4c_4$) precursor crystals obtained at a constant amount of 0.015 mol of NaSCN also accord perfectly with their offspring of MoS_2 hollow cages

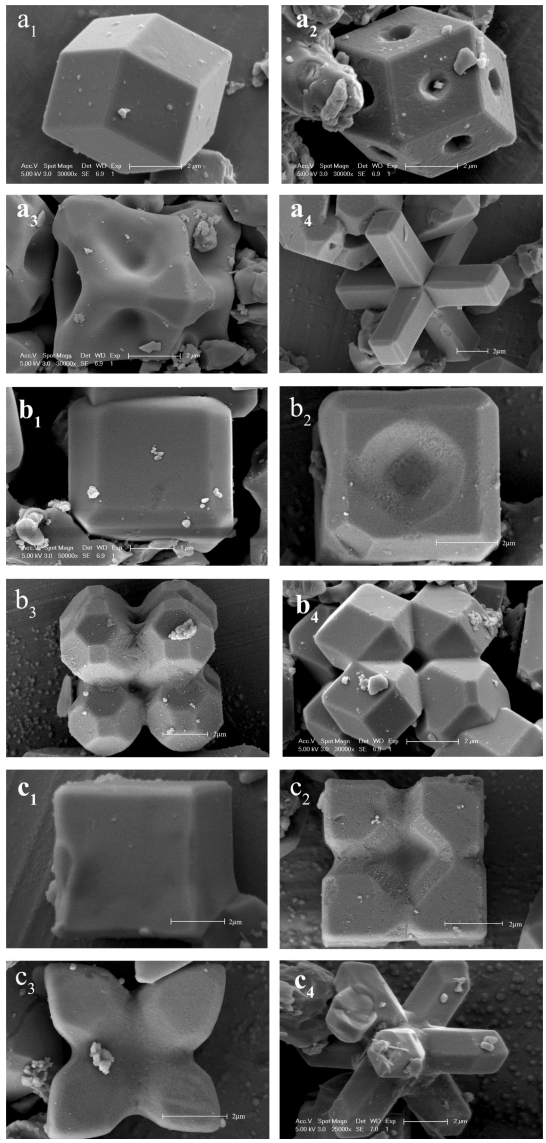

Figure 4. FESEM images of the precursor crystals fabricated at 160 °C for 8 h, from solutions of (a) a constant amount of 0.01 mol of NaSCN and varying amount of Bu_4NBr, of (a_1) 0.0009 mol of Bu_4NBr, (a_2) 0.00105 mol of Bu_4NBr, (a_3) 0.0012 mol of Bu_4NBr, and (a_4) 0.00128 mol of Bu_4NBr; (b) a constant amount of 0.012 mol of NaSCN and varying amount of Bu_4NBr, of (b_1) 0.0009 mol of Bu_4NBr, (b_2) 0.00098 mol of Bu_4NBr, (b_3) 0.00105 mol of Bu_4NBr, and (b_4) 0.0012 mol of Bu_4NBr; (c) a constant amount of 0.015 mol of NaSCN and varying amount of Bu_4NBr, of (c_1) 0.0012 mol of Bu_4NBr, (c_2) 0.0015 mol of Bu_4NBr, (c_3) 0.00165 mol of Bu_4NBr, and (c_4) 0.0018 mol of Bu_4NBr.

in Figure 1c. These FESEM observations confirm that these precursor crystals with smooth surface serve as template for the subsequent formation of various morphology-preserved MoS_2 hierarchical hollow cages. Despite their different morphologies, X-ray diffraction (XRD) investigation reveals that all the in situ formed precursor crystals show exactly identical XRD patterns, confirming the same substance. An XRD pattern (denoted by scattering vector $s = 2 \sin \theta/\lambda$ with 2θ being the scattering angle), which provides structure information for the as-captured in situ formed precursor crystals at 160 °C for 8 h, as shown in Figure 5, indicates that all the reflections of the XRD can be indexed on a body-centered-cubic cell with lattice constant of $a = 12.5$ Å. Well-resolved reflections allow them to be distinguished unam-

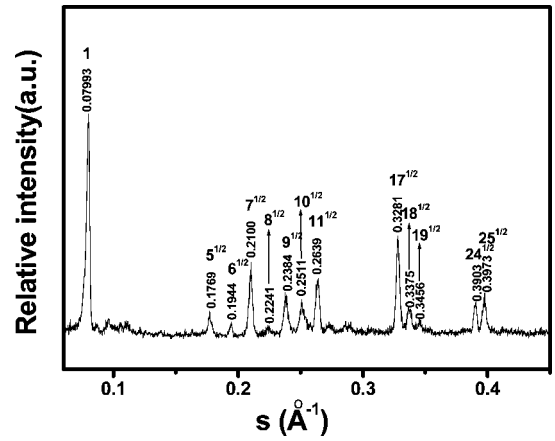

Figure 5. XRD pattern of the precursor crystals obtained at 160 °C for 8 h from the solution of 0.01 mol of NaSCN and 0.0009 mol of Bu_4NBr, the x-axis of which denotes the absolute value of the scattering vector $s = 2 \sin \theta/\lambda$ with 2θ being the scattering angle.

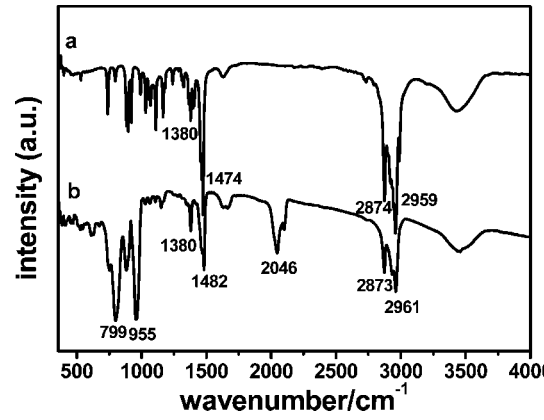

Figure 6. Fourier transform infrared (FTIR) spectra of (a) Bu_4NBr, (b) the precursor crystals obtained at 160 °C for 8 h with 0.01 mol of NaSCN and 0.0009 mol of Bu_4NBr. Some of the Bu_4NBr bands (2959, 2874, 1474, 1465, and 1380 cm^{-1}) could be seen clearly in Fourier transform infrared (FTIR) spectra of the precursor crystals, confirming the existence of Bu_4N^+. Two strong bands at 955 and 799 cm^{-1} in Fourier transform infrared (FTIR) spectra could be attributed to the Mo–O stretch vibration in molybdate.

biguously between body-centered and primitive cubic due to the presence of $7^{1/2}$ reflection.[10]

3.3. Exact Composition Characterization of the Precursor Crystals. The exact composition of the in situ formed precursor template was further investigated by other techniques, including X-ray fluorescence spectra (XFS), Fourier transform infrared (FTIR) spectra, X-ray photoelectron spectra (XPS), thermogravimetric analysis (TGA), elemental analysis, and inductively coupled plasma–atomic emission spectra (ICP-AES). Quasi-quantitative X-ray fluorescence spectra (XFS) of the precursor indicate the presence of C, N, Mo, O and rule out the presence of Br, Na, F, S. It is known that the Fourier transform infrared (FTIR) spectra is an effective approach to prove the existence of certain groups. As shown in Figure 6, some characteristic bands (2959, 2874, 1474, 1465, and 1380 cm^{-1}) belonging to the Bu_4NBr could be clearly seen in the Fourier transform infrared (FTIR) spectra of the precursor, confirming the existence of Bu_4N^+.

(10) (a) Liu, T.; Wan, Q.; Xie, Y.; Burger, C.; Liu, L. Z.; Chu, B. *J. Am. Chem. Soc.* **2001**, *123*, 10966–10972. (b) Chen, J.; Burger, C.; Krishnan, C. V.; Chu, B. *J. Am. Chem. Soc.* **2005**, *127*, 14140–14141.

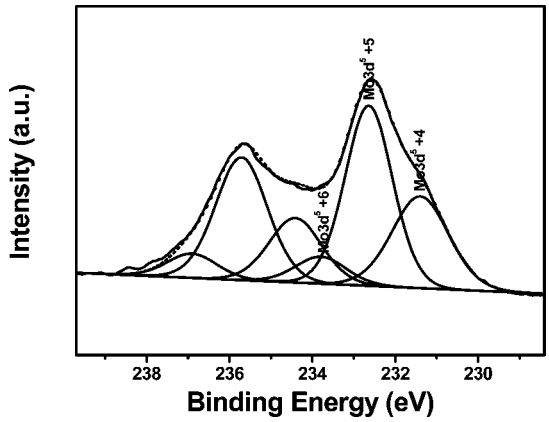

Figure 7. XPS Mo 3d spectra of the precursor crystals obtained at 160 °C for 8 h from the solution of 0.01 mol of NaSCN and 0.0009 mol of Bu_4NBr. XPS of all the precursor crystals are similar on the whole. Here the peaks of 231.4, 232.64, and 233.79 eV could be attributed to Mo(IV), Mo(V) and Mo(VI), respectively.

Meanwhile, two strong bands at 955 and 799 cm^{-1} could be attributed to the Mo–O stretch vibration in molybdate. Thus, FTIR spectra result clearly indicates the existence of $Bu_4N^+$and Mo oxo anions in the precursor crystals.

It is known that determining the oxidation state of the molybdenum atom is a prerequisite to knowing the exact composition of the Mo-involved compounds. The in situ formed precursors represent dark blue (the characteristic color for a mixture of Mo(IV), Mo(V), and Mo(VI)) rather than yellow (the characteristic color of Mo(VI)),[10] suggesting that the molybdenum components probably exist as a mixture of Mo(IV), Mo(V), and Mo(VI). The X-ray photoelectron spectra (XPS) of the sample (Figure 7) also provide the oxidation state information of the molybdenum atoms. It is reported that 1 eV can be added for each increase in oxidation from Mo metal (228 eV), and an emission at 232 eV has previously been attributed to MoO_2; thus, the peaks at 232–233 eV could be due to Mo(V).[11] Peak deconvolution indicates that the Mo $3d_{5/2}$ emission is constituted of three contributions: a major one at 232.64 eV and two smaller ones at 231.4 and 233.79 eV, which could be attributed to Mo(V), Mo(IV), and Mo(VI), respectively. The average oxidation state of the molybdenum atom can also be determined in the thermogravimetric analysis (TGA) curves (Figure 8) by comparing the weight loss difference recorded in argon atmosphere (final form: MoO_x) and air atmosphere (final form: MoO_3).[10b] When the intermediate precursor crystal was heated in argon, the oxidation state of Mo would not change during the heating process. Therefore, after the complete decomposition of $N(C_4H_9)_4^+$ at 500 °C, the oxidation state of Mo remained the same as it in the intermediate precursor crystal to form MoO_x. However, when the intermediate precursor crystal was heated in air, Mo would be oxidized by oxygen in air, and the oxidation state of Mo would rise to produce MoO_3 after the complete decomposition of $N(C_4H_9)_4^+$ at 500 °C. The relative weight gain of the transformation from MoO_x to MoO_3 corresponding to the relative weight loss difference in air and in argon[10b] is calculated to be 3.05%, from which we obtain a value of 2.6 for x. This mixed-valent oxidation state of IV, V, and VI corresponds to an average oxidation state of 5.2 for molybdenum. All the oxidation state information of the molybdenum atom implies that partial reduction of Mo(VI) to Mo(V) or Mo(IV) by S^{2-} ions released from SCN^- has taken place during the in situ formation process of precursor.

TGA measurements can also provide the composition information for the precursor; elemental analysis technique was used to characterize the intermediate products heated at a certain temperature. The thermal decomposition process of the precursor in an argon atmosphere shown in Figure 8a can be divided into two stages: In the first stage between 20 and ~200 °C, a mass loss of 1.95% is observed and attributed to the elimination of absorbed water during the heating process. In the second stage range from 200 to ~500 °C, a mass loss of 39.16% is observed and attributed to the loss of $N(C_4H_9)_4^+$ ions, and the remaining weight (58.89%) is assigned to $MoO_{2.6}$. Elemental analysis results confirm that the surfactant $N(C_4H_9)_4^+$ ions have been completely removed when heating the precursor at 500 °C for 2 h in an argon atmosphere. Calculating from the mass loss of $N(C_4H_9)_4^+$ (39.16%) and the remaining weight of $MoO_{2.6}$ (58.89%) leads to the empirical formula $[(C_4H_9)_4N]_{0.4}(MoO_{2.8})$, which requires a theoretical weight loss of 42.14% (the remaining substance is $MoO_{2.6}$) close to the observed one of 39.16% for $(C_4H_9)_4N^+$ from the TGA data. Analysis for $[(C_4H_9)_4N]_{0.4}(MoO_{2.8})$ gives for the theoretical values from the empirical formula (in wt %): Mo = 40.36, C = 32.34, N = 2.36, H = 6.1 which mainly matches with the experimental ones obtained from the result of inductively coupled plasma–atomic emission spectra (ICP-AES) and element analysis: Mo = 40.65, C =27.23, N = 2.14, H = 5.4. The experimental value of C is lower than the theoretical one, which is probably attributed to the incomplete combustion of carbon in the element analysis experiments. Element analysis gives further evidence that the empirical formula $[(C_4H_9)_4N]_{0.4}(MoO_{2.8})$ is credible.

3.4. Formation Mechanisms of the Precursor Crystals. Combined with XRD, XFS, FTIR, XPS, TGA, elemental analysis, and ICP-AES, the in situ formed precursor template is proved to be a composite of Mo oxo anion and tetrabutylammonium cation ($[(C_4H_9)_4N]_{0.4}(MoO_{2.8})$) with a body-centered-cubic cell. It is well-known that surfactant cation and metal oxo anion can co-organize to form periodic surfactant/inorganic composite materials if the charge density at the surfactant/inorganic interfaces matches well.[12] The formed surfactant/molybdate composite $[(C_4H_9)_4N]_{0.4}(MoO_{2.8})$ is similar to the periodic surfactant/inorganic composite materials reported by Stucky et al. on the basis of specific electrostatic interaction of surfactant headgroups (S) and inorganic species (I) in solution.[12] Our surfactant/molybdate composite forms by the cooperative assembly of periodic Mo oxo anion and tetrabutylammonium cation, involving the

(11) (a) Ozin, G. A.; Özkar, S.; Prokopowicz, R. A. *Acc. Chem. Res.* **1992**, *25*, 553–560. (b) Grim, S. O.; Matienzo, L. J. *Inorg. Chem.* **1975**, *14*, 1014–1018. (c) Antonelli, D. M.; Trudeau, M. *Angew. Chem., Int. Ed.* **1999**, *38*, 1471–1475.

(12) Huo, Q.; Margolese, D. I.; Ciesla, U.; Feng, P.; Gier, T. E.; Sieger, P.; Leon, R.; Petroff, P. M.; Schüth, F.; Stucky, G. D. *Nature* **1994**, *368*, 317–321.

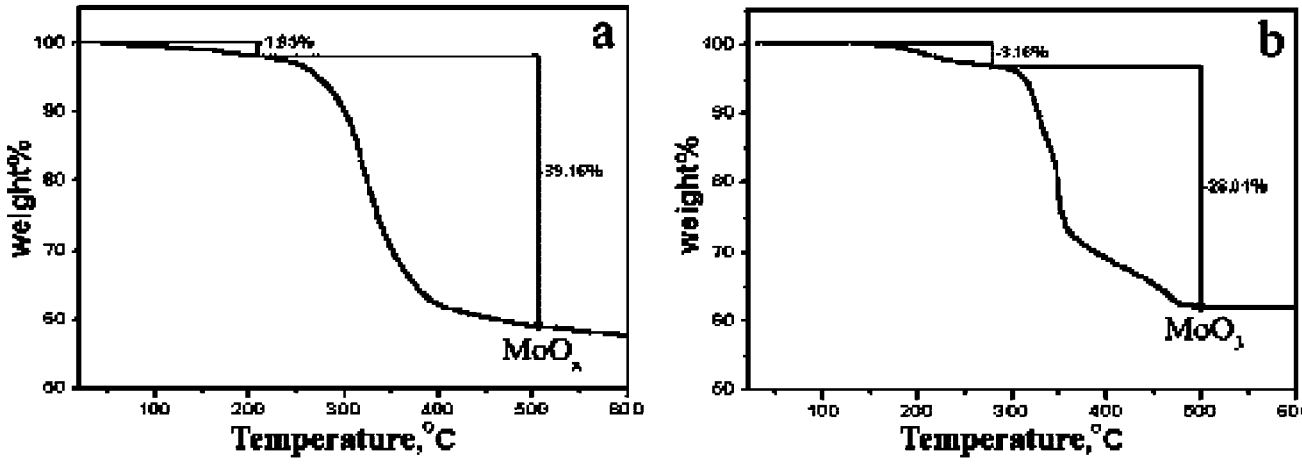

Figure 8. TGA curves of the precursor crystals obtained at 160 °C for 8 h from the solution of 0.01 mol of NaSCN and 0.0009 mol of Bu_4NBr: (a) recorded in an argon atmosphere; (b) recorded in air.

direct co-condensation of anionic inorganic species with a cationic surfactant (S^+I^-).[12]

In the process of the formation of the precursor template, F^- ions can enhance the dissolution and reaction of MoO_3 by nucleophilic substitution,[13] and S^{2-} ions, which are released from SCN^- upon a hydrolyzation process, serve as the reducing agent. The whole reaction process can be expressed as follows:

$$2MoO_3 + 2F^- \rightarrow MoO_4^{2-} + MoO_2F_2 \quad (1)$$

$$MoO_2F_2 + 2H_2O \rightarrow MoO_4^{2-} + 2F^- + 4H^+ \quad (2)$$

$$10MoO_4^{2-} + S^{2-} + 8H_2O + 4(C_4H_9)_4N^+ \rightarrow 10[C_4H_9]_{0.4}(MoO_{2.8}) + SO_4^{2-} + 16OH^- \quad (3)$$

The final MoS_2 forms in the sulfuretted process of precursor crystals at 220 °C, in which S^{2-} that is released from SCN^- upon a hydrolyzation process serves as reducing agent and sulfur source; thus, the in situ formed precursor crystals with adjustable morphology are able to act as both Mo source and self-sacrificed template for the subsequent formation of various morphology-preserved MoS_2 hierarchical hollow cages based on the Kirkendall effect.[7] The reaction could be expressed as follows:

$$20[(C_4H_9)_4N]_{0.4}(MoO_{2.8}) + 43S^{2-} + 44H_2O \rightarrow 20MoS_2 + 3SO_4^{2-} + 8(C_4H_9)_4N^+ + 88OH^- \quad (4)$$

3.5. Effects of the Reaction Conditions on the Morphology of Precursor Crystals. The in situ formed precursor template crystals with various well-defined morphologies, as shown in Figure 4, clearly reveal that the SCN^- concentration and surfactant concentration in turn determine the morphologies of precursor crystals. In our study, the amount of NaSCN decides the basic crystal habit of the precursor crystals that is determined by the relative order of different surface energies. It is well-known that higher surface energy faces tend to grow along its normal direction and eventually disappear from the final appearance, while lower surface energy faces increase in area.[14–16] Addition of inorganic or organic additives to the reaction during the crystal growth may modify the relative order of different surface energies; that is, the preferential absorption of molecules and ions in solution on different crystal faces lowers the surface energy of the bound plane and hinders the crystal growth along the normal direction of the plane, directing the growth of nanoparticles into various shapes.[14,15] In the present case, the formation of rhombododecahedral habit, 18-face polyhedral habit, and cubic habit for the precursor crystals with mostly exposed {110} or {100} faces is due to the large differences between their growth rates and that for {111} faces. Relatively faster growing {111} faces disappear from the final appearance, but more stable {100} and {110} faces will become mostly exposed. Under the lower amount of NaSCN (0.01 mol), precursor crystals growing as rhombododecahedral habit with mostly exposed {110} faces reveals that the surface energy of {110} faces is the lowest among the two kinds of faces {100} and {110}, resulting in the slowest crystal growth along the ⟨110⟩ direction. When the NaSCN amount increases, the growth habit of precursor crystals changing from rhombododecahedral with mostly exposed {110} faces to cubic with mostly exposed {100} faces, implies that the surface energy of {100} faces becomes the lowest among the two kinds of faces {100} and {110}, resulting in the slowest crystal growth along the ⟨100⟩ direction at higher amount of NaSCN (0.015 mol). The change of the growth habit further exhibits evident preferential adsorption of SCN^- onto the {100} faces of the precursor crystals. This adsorption on the {100} faces lowers the surface energy of the {100} faces and selectively hinders crystal growth along the ⟨100⟩ direction, resulting in the increase of the surface energy and the growth rate differences between the {100} and {110} faces. The relatively faster growth rate for {110} faces will result in the diminishing of these faces, but more stable {100} faces will become mostly exposed to produce 18-face polyhedral habit and cubic habit

(13) Yu, J.; Yu, J. C.; Ho, W.; Wu, L.; Wang, X. *J. Am. Chem. Soc.* **2004**, *126*, 3422–3423.
(14) Cao, H.; Qian, X.; Wang, C.; Ma, X.; Yin, J.; Zhu, Z. *J. Am. Chem. Soc.* **2005**, *127*, 16024–16025.
(15) Siegfried, M. J.; Choi, K.-S. *Adv. Mater.* **2004**, *16*, 1743–1746.
(16) Siegfried, M. J.; Choi, K.-S. *Angew. Chem., Int. Ed.* **2005**, *44*, 3218–3223.

as the amount of NaSCN increases. Our earlier work[7] observed similar phenomena, that is, only irregular $K_2NaMoO_3F_3$ polyhedrons can be obtained without the existence of SCN^-, while the presence of SCN^- promotes the formation of intermediate $K_2NaMoO_3F_3$ crystals with cubic shape, further confirming the preferential absorption ability of SCN^- on certain crystal facets.

Branching growth has been proposed to be determined by a diffusion effect.[16–18] Crystal consumes ions or molecules near the surface as it grows, and a concentric diffusion field forms around the crystal; meanwhile, branching forms as the apexes of a polyhedral crystal, which protrude further into the region of higher concentration, grow faster than the central parts of facets.[16] It has been accepted that the change of experimental conditions, such as voltage, electrical current,[16] temperature, and concentration,[19] is readily to affect the diffusion effect. For example, through slight changes in temperature and humidity, snow crystals can grow into different morphologies with varying degrees of branching.[19] Our present work indicates that branching of precursor crystals is extremely sensitive to the concentration of Bu_4NBr; that is, the higher concentration of Bu_4NBr, the clearer branching of the formed precursor crystals. Under the lower amount of NaSCN (0.01 mol), crystals of rhombododecahedron, rhombododecahedron with a total of 12 intracrystal holes on the centers of {110} planes, enlarged hexapod, and hexapod can be produced (Figure 4a), separately, as the concentration of Bu_4NBr increases. With an increase in the amount of NaSCN (0.012 mol), crystals of 18-face polyhedron, 18-face polyhedron with a total of six intracrystal holes on the centers of {100} planes, octa-18-face polyhedron interconnected by {100} facet sharing, and octa-rhombododecahedron interconnected by {100} facet sharing can be obtained (Figure 4b) as the concentration of Bu_4NBr increases. At even higher amount of NaSCN (0.015 mol), cubic, dicelike (cube with a total of six intracrystal holes on the centers of {100} planes), enlarged octapod, and octapod crystals can be fabricated (Figure 4c) as the concentration of Bu_4NBr increases. All of the experimental results shown in Figure 4 confirm that it is the increase in the concentration of Bu_4NBr which causes an increase in diffusion effect that affects the degree of branching of the precursor template crystals. These morphology evolution processes are schematically shown in Scheme 1, representing that, with increase in the concentration of Bu_4NBr, the degree of branching of the precursor crystal also increases, regardless of the initial growth habit. All these novel morphologies of precursor crystals are undoubtedly good candidates for further self-sacrificed template for the final MoS_2 hierarchical hollow cages.

Scheme 1. Branching of the Precursor Crystals of Different Habit with the Increase of the Concentration of Bu_4NBr: (a) Rhombododecahedral Habit Crystals; (b) 18-Face Polyhedral Habit Crystals; (c) Cubic Habit Crystals

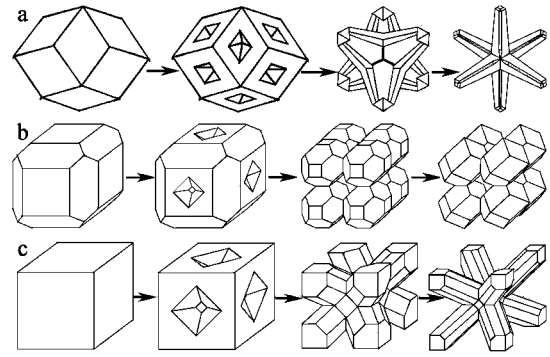

4. Conclusions

In summary, we proposed a general route to MoS_2 hierarchical hollow cages, in which abundant hollow cages with various well-defined, novel geometrical morphologies were fabricated via a self-assembly coupled with surfactant/molybdate composite precursor crystal templating process based on the Kirkendall effect. The in situ formed surfactant/molybdate composite precursor crystals with cubic structures, which are cooperatively assembled by periodic Mo oxo anion and tetrabutylammonium cation, play crucial roles as both the Mo source and the template in the formation of MoS_2 hierarchical hollow cages. The surfactant/molybdate composite precursor crystals with different morphologies were controllably synthesized through a methodical tuning of the habit and the degree of branching of precursor crystals by varying the SCN^- concentration and surfactant concentration. Furthermore, the synthesis may be extended to other sulfide systems and could be used for device fabrication with appropriate surfactant/inorganic composite precursor/sulfur source combinations.

Acknowledgment. This work was supported by the National Nature Science Foundation (NSF) of China (No. 20621061) and the state key project of fundamental research for nanomaterials and nanostructures (2005CB623601).

Supporting Information Available: XRD pattern of the final product of MoS_2 hierarchical hollow cages. This information is available free of charge via the Internet at http://pubs.acs.org.

CM702007F

(17) Chernov, A. A. *J. Cryst. Growth* **1974**, *24/25*, 11–31.
(18) Kudora, T.; Irisawa, T.; Ookawa, A. *J. Cryst. Growth* **1977**, *42*, 41–46.
(19) Yokoyama, E.; Kudora, T. *Phys. Rev. A* **1990**, *41*, 2038–2049.